(Received 14 April 2024, Accepted 31 May 2024, Scheduled 14 June 2024)

A Low Profile Wideband Circularly Polarized Patch Antenna Using Metasurface

Yongkang Yuan, Minquan Li*, Guocui Zhu, Xin Qu, and Zhonghui Li

Information Materials and Intelligent Sensing Laboratory of Anhui Province, Anhui University, Hefei 230039, China

ABSTRACT: A low profile, wideband circularly polarized (CP) antenna using metasurface (MS) is proposed. The proposed antenna is composed of a square loop feeding structure and four driven patches positioned between the ground plane and the MS. First, the loop with truncated corners functions as a sequential phase feeder for the four driven patches. These patches are then capacitively coupled by the feeding loop to create a CP mode. Then a defective ground structure (DGS) is adopted to improve the impedance matching. Finally, using MS to generate extra CP minimum AR points to broaden the AR bandwidth. The MS is composed of a 4×4 truncated square patch array which enhances the impedance bandwidth and gain of the proposed antenna. The total dimensions of the proposed antenna are $50\,\text{mm} \times 50\,\text{mm} \times 3.124\,\text{mm}$ ($\lambda_0 \times \lambda_0 \times 0.062\lambda_0$). The MS antenna in circular polarizations achieves a wide -10 dB impedance bandwidth of 37.5% (4.85–7.09 GHz) and a 3 dB axial ratio bandwidth (ARBW) of 20% (5.66–6.92 GHz). In addition, the maximum gain of 10.28 dBi is achieved at 6.1 GHz, and the proposed MS antenna also has a flat gain across a broad frequency range from 4.5 GHz to 6.75 GHz.

1. INTRODUCTION

The advancement of wireless communication systems has indeed increased the focus on circularly polarized antennas, particularly for their ability to reduce multipath interference and ensure reliable signal transmission and reception [1–3]. Microstrip patch antennas are also gaining attention due to their compact form and ease of integration into various devices [4]. Recognizing the respective advantages of circularly polarized and microstrip antennas, the current trend in antenna design leans towards developing circularly polarized patch antennas. These antennas combine the compactness and integrability of microstrip technology with the improved bandwidth and gain characteristics of circular polarization. This makes them highly suitable for modern communication systems such as Wireless Local Area Networks (WLAN) and Global Navigation Satellite Systems (GNSS).

Sequential Phase (SP) feeding technology, recognized for its ability to generate circular polarization radiation, has become a cornerstone in modern antenna design. It has been proposed in [5–7] that it can generate broadband circular polarization radiation. This technology's essence lies in the ability to produce circularly polarized radiation by stimulating two orthogonal modes that have a 90° phase difference, a fundamental principle for achieving circular polarization. In [7, 8], on the basis of sequential phase feeding, the structure of combined driven patches which excite circularly polarized resonant modes was adopted. In [7], 26.5% of the axial ratio (AR) bandwidth and 43.2% of the impedance bandwidth (IBW) are achieved through this structure. In [8], four surrounding patches served as driven patches are introduced to broaden the AR bandwidth of the antenna and generate one CP mode. Additionally, addressing the challenge of the 3 dB bandwidth limitation in circular polarization, the application of DGS has been explored as a means to increase the bandwidth for microstrip patch antennas. As shown in [9], this method not only augments the antenna's bandwidth but also keeps the antenna miniaturized.

Metasurfaces (MSs), the two-dimensional counterparts of metamaterials, have revolutionized antenna design by enhancing performance characteristics such as gain, impedance bandwidth, and polarization conversion from linear to circular polarization (LP to CP) [10]. As MS theory advances and its application broadens, antennas integrated with MS have begun to exhibit broadband capabilities even within low-profile designs, marking a significant leap forward in antenna technology. As shown in [11, 13, 14], by using MS, it is possible to improve the performance of antennas in low profile configurations. In [10], by truncating the unit cells of the MS, performance of the antenna has been improved in terms of AR and impedance bandwidth.

In this paper, a circularly polarized microstrip patch antenna based on MS is proposed. The square loop feeding structure and four driven patches are initially proposed to generate resonances and CP modes. Subsequently, with the application of the MS, both the impedance and AR bandwidth of the antenna are broadened. In addition, introducing DGS can further broaden the impedance bandwidth by generating additional resonances. The proposed antenna has low profile and is easy to integrate, with characteristics such as broadband and plat gain. Especially, the antenna combines the features of low profile and flat gain. It not only saves system space but also improves communication quality. This antenna is particularly suitable for

* Corresponding author: Minquan Li (limq@ahu.edu.cn).

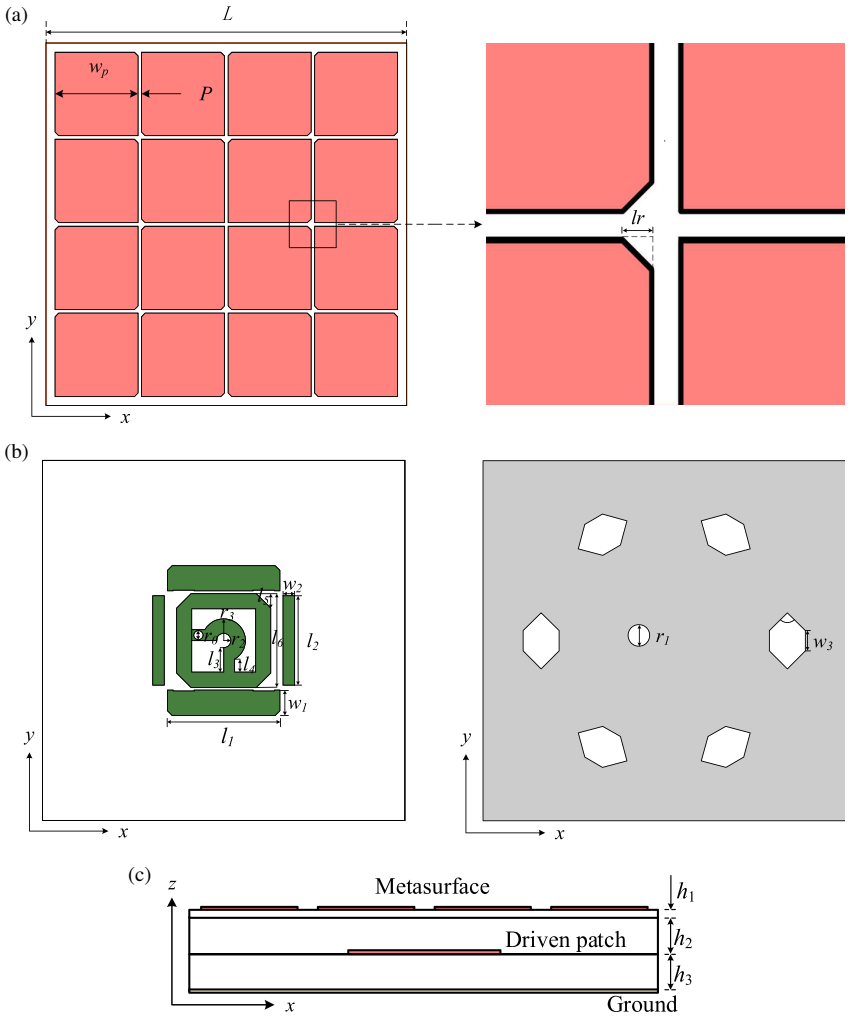

FIGURE 1. Geometry of the proposed antenna. (a) MS. (b) Top view of the radiation patches and ground plane. (c) Side view.

scenarios that require space savings without sacrificing communication quality, such as public transportation systems and commercial drones. This paper uses ANSYS High Frequency Structure Simulator (HFSS) for simulation, and the measurement results are generally consistent with the simulation ones.

2. ANTENNA DESIGN

2.1. Antenna Configuration

The proposed design for the broadband circularly polarized antenna, as shown in Fig. 1, incorporates several critical components for enhanced performance. The antenna's structure consists of a square loop feeding structure, four driven patches, MS, a ground plane, an SMA connector, low-loss dielectric foam, and is constructed using Rogers 5880 ($\varepsilon_r = 2.2$, $\tan\delta = 0.0009$) and Taconic FF-26D ($\varepsilon_r = 2.6$, $\tan\delta = 0.0011$) substrate. The square loop on the Rogers 5880 substrate serves as a feeding network. To facilitate a compact design and ease of integration, the construction eschews any air gap between the boards across all levels. The MS, placed atop the uppermost dielectric substrate, extends the antenna's impedance and AR bandwidth. The MS comprises 16 truncated square metal plates arranged in a 4×4 grid, with a consistent gap g, maintained between adjacent plates. The DGS used in this article consists of six hexagons etched on the ground, rotating sequentially around the center of the ground at an angle of 60°. The SMA connector's external segment connects to the ground plane, while its internal portion ascends through the Rogers 5880 substrate, di-

TABLE 1. Parameter of the antenna (unit: mm).

Parameter	Value	Parameter	Value
l_1	15.5	l_2	12.4
l_3	3.4	l_4	1.8
l_5	0.65	l_6	13
l_r	0.5	r_0	1.3
r_1	3	r_2	1
r_3	3	w_1	3.5
w_2	1.6	w_3	2.8
w_p	11.5	P	0.5
h_1	0.1	h_2	1.5
h_3	1.524	L	50

rectly linking to the square loop at its feed point. The design's dimensions and configurations, depicted in Figs. 1(a) to 1(c), were refined using ANSYS HFSS 15.0, with specific parameters detailed in Table 1.

2.2. Design Process

Firstly, before designing the radiation patch of the proposed antenna, determine the use of the MS and DGS. Suitable MS and defect ground structures have been determined through multiple simulations. The MS comprises 16 truncated square metal plates arranged in a 4×4 grid, with a consistent gap g, maintained between adjacent plates. The DGS is intricately designed, featuring six hexagons etched into the ground plane. These hexagons are strategically rotated around the center at precise 60° intervals, enhancing the antenna's performance by influencing the distribution and flow of surface currents.

After determining the MS and DGS, we began to focus on the design of radiation patches. The proposed antenna is centered at a frequency of 6.0 GHz, utilizing a corner-truncated square loop structure in the feeding network. This setup incorporates two pairs of driven patches positioned externally to the square loop feeder, each exhibiting sequential phase characteristics. Initially, a 90° phase difference is achieved through an arc-shaped delay line within the square loop. To broaden the impedance bandwidth, four driven patches are then arranged around this loop. Enhancing the antenna's performance further, six hexagonal slots are etched into the ground plane. The role of the MS, explained in detail in [6] and [11], involves its placement at the antenna's top layer to augment both AR bandwidth and gain. To compact the antenna's size while preserving its impedance and axial ratio bandwidth, no air gap is introduced between the driven patches and the MS. Instead, a layer of low dielectric loss foam is inserted between them. For a clearer understanding of the design evolution, Fig. 2 presents three prototypes. Prototype Ant.1 features a feeding loop printed on a Rogers 5880 substrate, with an arc-shaped strip in the loop creating a 90° phase difference. This setup divides the loop's fundamental wavelength mode into two orthogonal, nearly degenerate modes, achieving a CP mode. Building upon Ant.1, Ant.2 adds two driven patches on opposite sides of the loop feeder. These corner-truncated patches, equipped with slots, are closely coupled to the loop feeder, introducing a new resonant mode. As illustrated in Figs. 3(a) and (b), this addition not only improves impedance matching over Ant.1 but also shifts resonance points to a lower frequency band, with the minimum AR point moving towards higher frequencies. For Ant.3, by integrating two additional driven patches to the remaining sides of the loop feeder, the design treats the loop's four sides which serve as ports, each coupling equal feed signals with phase shifts of 0°, 90°, 180°, and 270° to the four driven patches, thereby generating multiple AR minimum points across the frequency band.

FIGURE 2. Design process of the proposed antenna.

2.3. Operation Mechanism

As shown in Fig. 1(a), the MS used in this article is composed of 16 square metal plates arranged in a 4×4 grid and separated by consistent gap P. To enhance the performance of the antenna in generating circular polarization, the corner of each square metal patch is truncated. The truncation of these square plates not only widens the gap between adjacent and relative elements, but also plays a crucial role in the overall performance of the antenna by affecting two key parameters: the equivalent capacitance and phase difference between elements. Firstly, by truncating corners, the physical spacing between adjacent metal plates can be increased, effectively reducing their equivalent capacitance. The electric field interaction between capacitors and adjacent plates is directly related. Therefore, increasing the gap reduces the capacitance effect. This reduction in capacitance can affect the resonant frequency of the antenna, potentially widening the bandwidth and allowing for more flexible adjustment of the antenna's response to different frequencies. In addition, truncating corner can also cause changes in phase difference: the change in phase difference between metal patches is a direct result of the electric field interaction that changes due to the increase in gap. The phase of the electromagnetic waves reflected or transmitted by each unit can be finely controlled by the geometric shape of the MS. By carefully designing these truncation angles, the phase difference on the element surface can be manipulated to achieve the desired circular polarization.

As shown in Fig. 1(b), six hexagon slots are etched on the ground plane and are strategically rotated around the center at precise 60° intervals. This rotation not only aids in managing the antenna's directivity and bandwidth but also contributes to the suppression of unwanted frequencies, thereby refining the overall efficiency and operational bandwidth of the antenna. In order to demonstrate that incorporating a defective ground structure can enhance the impedance characteristics of an antenna, Fig. 4 presents a comparative graph of $|S_{11}|$ before and after loading of DGS. As illustrated in the figure, the addition of DGS to the antenna results in an increase in effective resonance points and a broadening of the bandwidth. This modification substantively improves the antenna's performance by optimizing its impedance properties.

To effectively showcase the capabilities and functioning of the proposed circularly polarized patch antenna, Fig. 2 displays three progressively developed antenna prototypes (Ant.1-Ant.3). Fig. 3 presents the impedance bandwidth, AR bandwidth, and gain for each prototype. Ant.1 features a loop feeding network that creates a circular polarization pattern, facilitated by an arc-shaped delay line within the square loop structure. This design choice is critical for achieving circular polarization. The fundamental resonance mode (TM_{11} mode) of the ring antenna is activated at the operating frequency, specifically

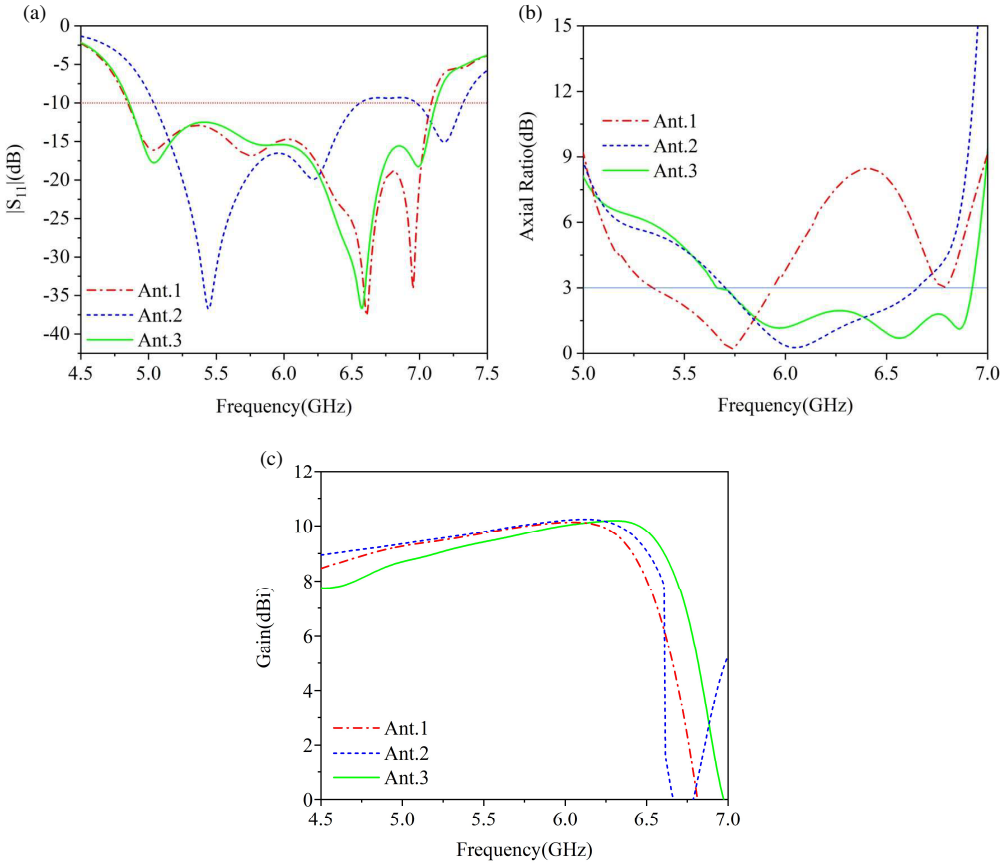

FIGURE 3. Comparison of different antennas. (a) $|S_{11}|$, (b) AR and (c) gain.

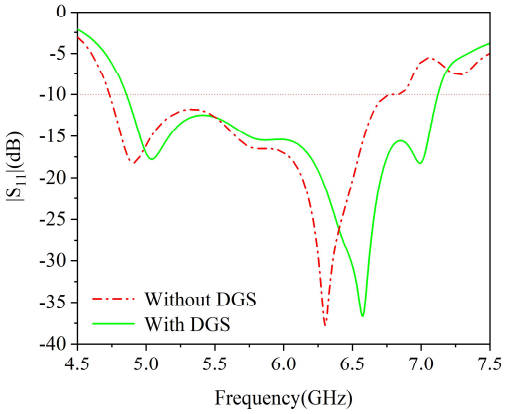

FIGURE 4. Comparison of $|S_{11}|$ before and after loading of DGS.

when the average circumference of the ring antenna closely matches the wavelength corresponding to the effective dielectric constant of the feed. The resonance frequency of this fundamental mode (TM_{11} mode) is dictated by the average circumference of the square ring and is a pivotal factor in the antenna's design, ensuring optimized performance at the desired frequency, which can be expressed as [15].

$$f_{11} = \frac{c}{2(l_1 + l_2)} \times \left(\frac{1 + \varepsilon_r}{2\varepsilon_r}\right)^{1/2} \quad (1)$$

where c represents the speed of light in free space; l_1 and l_2 are the inner and outer length of the square-ring respectively; $2(l_1 + l_2)$ is the mean circumference of the loop antenna; ε_r is the dielectric constant of the substrate; and f_{11} is the fundamental resonant frequency of the square-ring antenna.

As shown in Fig. 3(b), Ant.1 produces two minimum AR points at 5.75 and 6.75 GHz. When the two corner-truncated driven patches are arranged, Ant.2 produces two minimum AR points at 6.05 and 7.25 GHz. From this, it can be seen that after adding two corner-truncated driven patches, while increasing a resonance point, the minimum AR point also migrates towards the lower frequency region. To better illustrate the circular polarization performance of the antenna, Fig. 5(a) shows the radiation pattern of the central frequency point of the AR bandwidth of the antenna. Fig. 5(b) shows the AR pattern of the antenna at the central frequency point. As shown in the figure, with the θ changing, the AR remains at a value of 1.94 dB. This better demonstrates the circular polarization ability of the antenna. As shown in Fig. 3(c), the peak gains of the antennas with and without driven patches are 10.28 and 9.8 dBi.

Different frequencies tend to stimulate different circular polarization patterns. Therefore, in order to more accurately understand the generation mechanisms of the wideband circularly polarized radiation, simulated surface current distributions of the radiation patches at 6.0, 6.6 GHz (due to the gain approaching zero at 6.8 GHz, the current distribution at this frequency

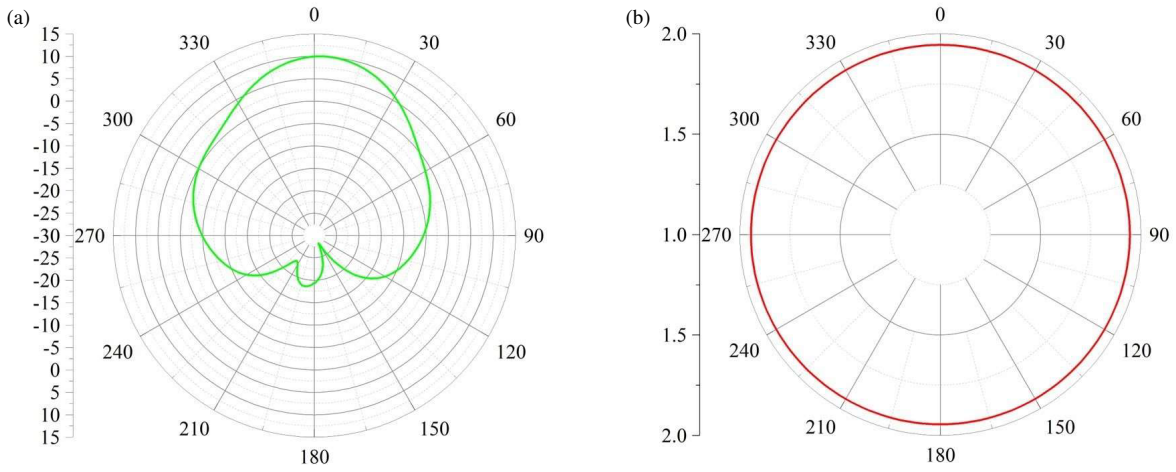

FIGURE 5. (a) Radiation pattern at 6.29 GHz, (b) AR pattern at 6.29 GHz.

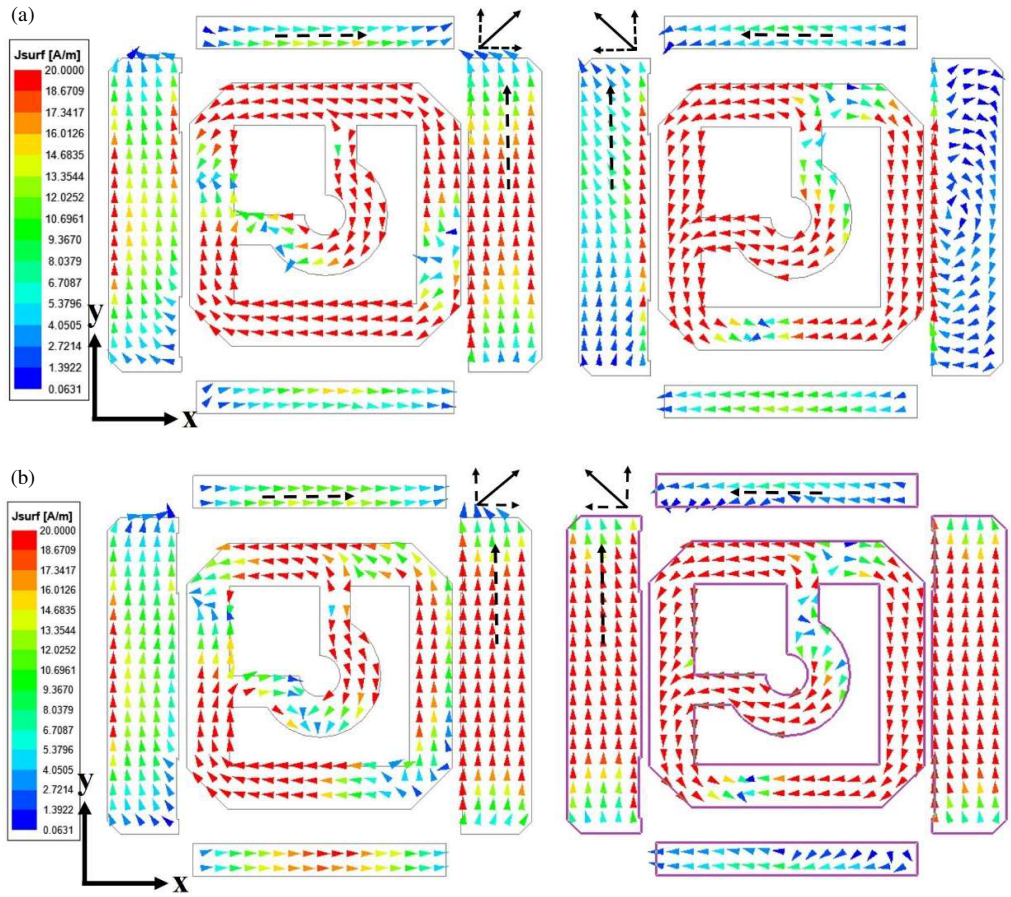

FIGURE 6. Surface current distributions of the radiation patches at (a) 6.0 and (b) 6.6 GHz.

point is not analyzed) are depicted in Fig. 6. At 6.0 GHz, it is shown that the directions of the square loop are the same at 0° phase and 90° phase, while the currents on the two pairs driven patches are orthogonal. For 0° phase, the sum of vector current on the driven patches sequentially rotates through angles of 45° relative to the $+x$ axis. While at 90° phase, the sum of vector current on the driven patches sequentially rotates through angles of $-45°$ relative to the $+x$ axis. Therefore, all the driven patches are CP at 6.0 GHz. Fig. 6(a) indicates that the resonance observed at 6.0 GHz is predominantly determined by the characteristics of the four driven patches, suggesting that the proposed antenna achieves circular polarization through driven elements that are linearly polarized (LP). At 6.6 GHz, because the driven patches are coupled by loop feeding network with

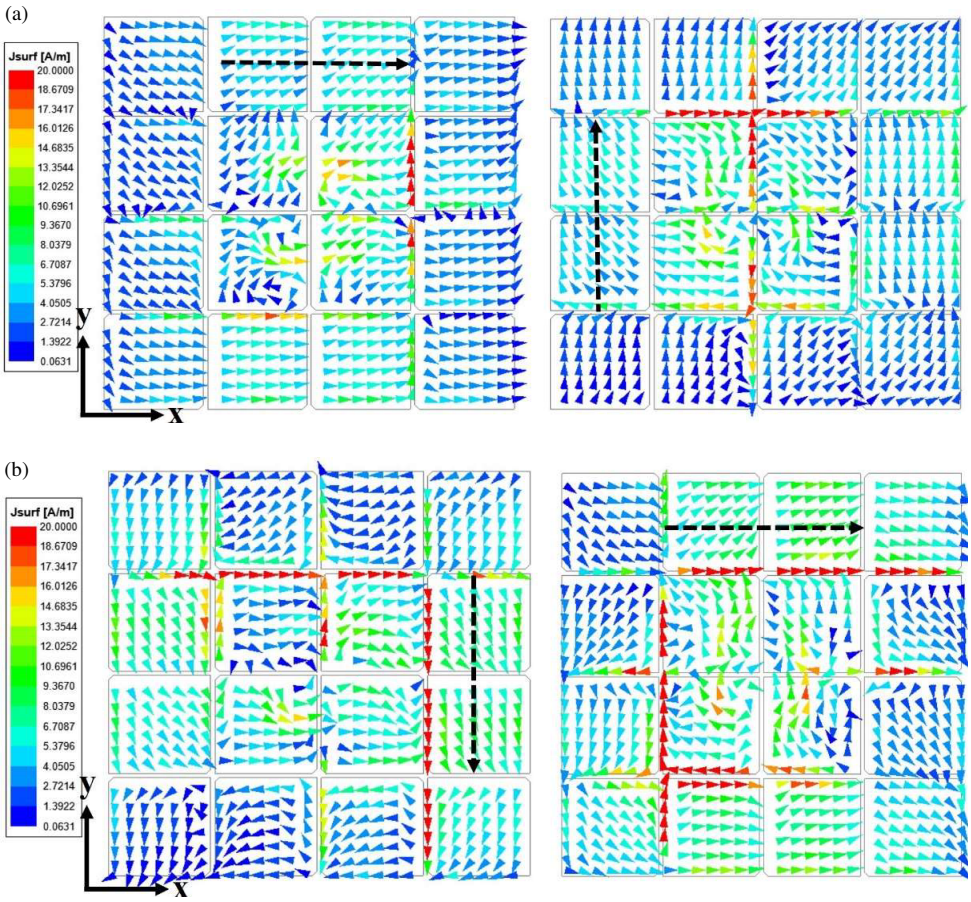

FIGURE 7. Vector current distributions on the MS of the 4×4 cells configuration for different phase angles: (a) 6.0, (b) 6.6 GHz.

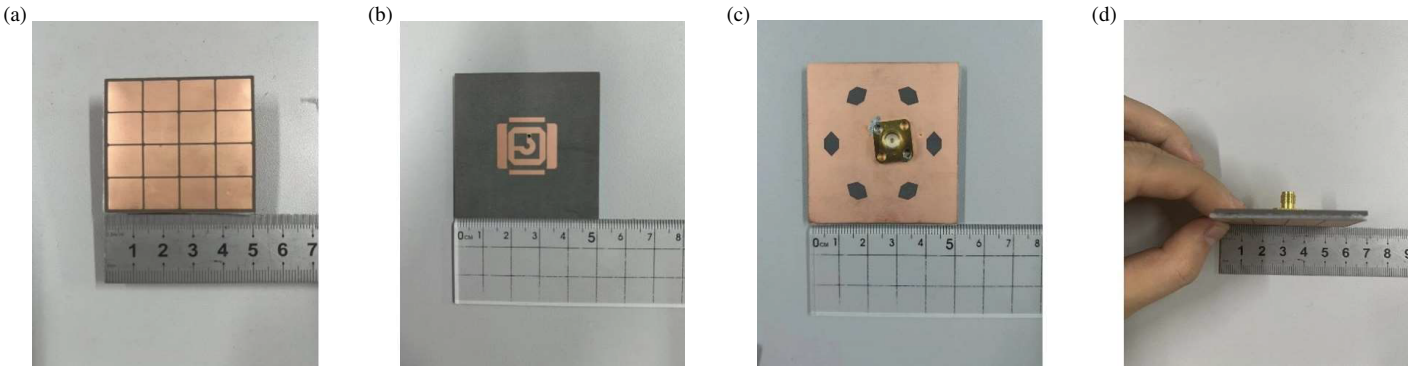

FIGURE 8. Photograph of the fabricated prototype. (a) Top view of the MS, (b) top view of the radiation patches, (c) ground plane, (d) side view of the antenna.

the phase difference of 90°, two pairs driven patches are simultaneously excited. At 0° phase, similar to the 6.0 GHz, the dominant current is 45° with respect to $+x$ axis direction while it rotates to $-45°$ with respect to $+x$ axis direction at the phase of 90°. Therefore, the driven patch is CP at 6.6 GHz.

Next, analyzing the current distribution on MS is also crucial. As shown in Fig. 7(a), when the frequency is 6.0 GHz, the direction of the dominant current on the MS is $+x$ at the phase of 0° whereas the direction of the dominant current of the MS is $+y$ at the phase of 90°. When the frequency is 6.6 GHz, the direction of the dominant current of the MS is $-y$ at the phase of 0°, whereas the direction of the dominant current of the MS is $+x$ at the phase of 90°. It is demonstrated that at each point where the axial ratio (AR) reaches its minimum, two orthogonal modes are excited with a 90° phase difference to produce additional circularly polarized (CP) radiation.

Moreover, as shown in Figs. 7(a) and (b), at 6.6 GHz, the currents on the metal surface (MS) were more intense than those at

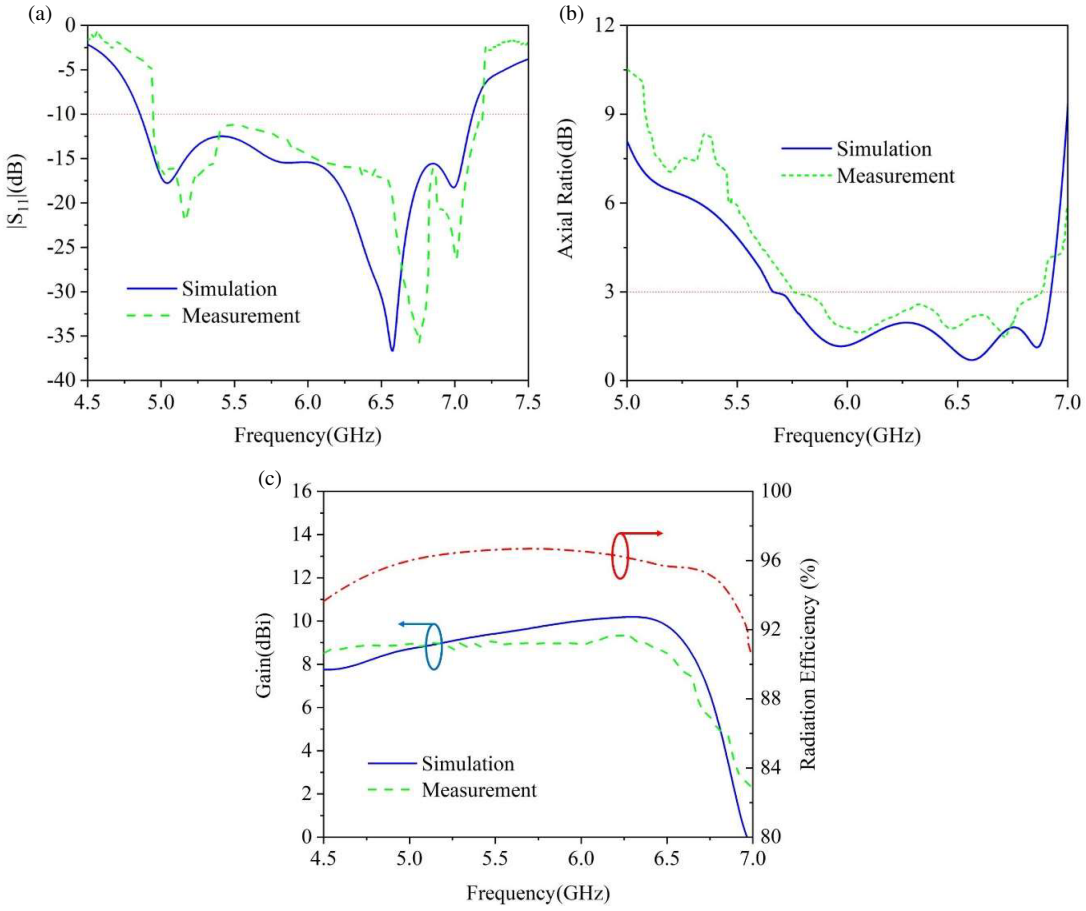

FIGURE 9. (a) $|S_{11}|$, (b) AR and (c) gain and radiation efficiency.

TABLE 2. Comparison of the proposed antenna to previously reported antennas.

Ref.	Size (λ_0^3)	MS	Number of layers	IBW (%)	AR (%)	Max. Gain (dBi)	Radiation efficiency (%)	Type of polarization
[5]	$1.45 \times 1.45 \times 0.028$	No	1	15.9	11.8	12.5	N/A	RHCP
[6]	$1.02 \times 1.02 \times 0.028$	No	1	25.8	20.6	8 (dBic)	N/A	RHCP
[8]	$0.92 \times 0.92 \times 0.028$	No	1	19.5	12.9	9.8	90	RHCP
[12]	$1.5 \times 1.5 \times 0.6$	No	1	20.8	17.6	11.5	N/A	LHCP/RHCP
[13]	$1.1 \times 1.1 \times 0.093$	Yes	2	34.7	20.1	11 (dBic)	N/A	LHCP
[14]	$1.16 \times 1.16 \times 0.067$	Yes	2	21	14.9	9.3	N/A	RHCP
[16]	$1 \times 1 \times 0.07$	Yes	2	28.2	20.9	9.7 (dBic)	88	LHCP
[17]	$1.14 \times 1.14 \times 0.05$	Yes	1	18.6	18.6	5	60	RHCP
[18]	$1.44 \times 0.9 \times 0.35$	Yes	2	48.45	19.67	8.75 (dBic)	80	LHCP/RHCP
[19]	$0.47 \times 0.47 \times 0.09$	No	2	17.9	11	7.1 (dBic)	N/A	LHCP/RHCP
[20]	$0.78 \times 1.37 \times 0.03$	No	1	33.4	19.3	6.6	88	LHCP
[21]	$0.63 \times 0.63 \times 0.042$	No	3	8	5	6.19	N/A	LHCP/RHCP
[22]	$0.56 \times 0.56 \times 0.076$	Yes	2	21.52	12.78	13.4 (dBic)	93	CP
[23]	$1 \times 1 \times 0.052$	Yes	1	20.18	16.21	10.43 (dBic)	N/A	RHCP
[24]	$0.79 \times 0.79 \times 0.029$	No	2	N/A	12.5	9.4 (dBic)	N/A	RHCP
Proposed	$1 \times 1 \times 0.062$	Yes	2	37.5	20	10.28	90	RHCP

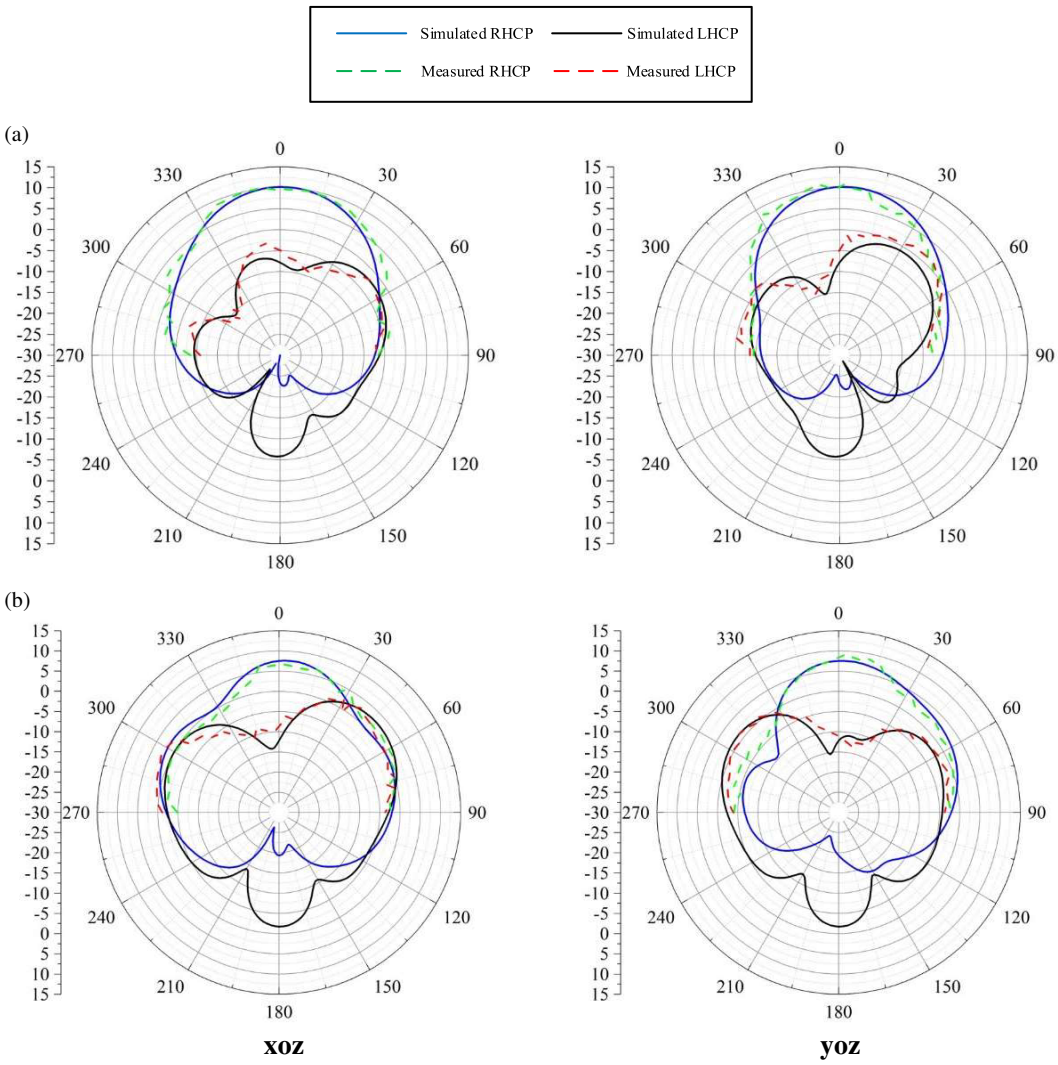

FIGURE 10. Simulated and measured antenna radiation patterns. (a) 6.0 GHz, (b) 6.6 GHz.

6.0 GHz. Specifically, at 6.0 GHz, the strongest currents were localized in the center of the MS, whereas at 6.6 GHz, the highest currents were distributed across all the metal plates. This distribution indicates that the point of minimum AR at 6.6 GHz is primarily influenced by the MS.

3. MEASUREMENT RESULTS

To validate the effectiveness of the proposed design, the antenna was fabricated and subsequently tested. The complete proposed antenna is depicted in Fig. 8. A vector network analyzer was utilized to evaluate the impedance bandwidth ($|S_{11}|$) of the antenna. Fig. 9(a) presents a comparison between the measured and simulated $|S_{11}|$ values. According to the data, the measured impedance bandwidth, where $|S_{11}| < -10$ dB, spans from 4.9 GHz to 7.2 GHz, accounting for a 38% range. Notably, the measured bandwidth is broader than that predicted by simulations, likely due to variations introduced during the manufacturing process.

Furthermore, the AR and gain of the antenna were also measured and simulated, with the results displayed in Figs. 9(b) and (c). These measurements were carried out in a microwave anechoic chamber, ensuring accurate assessment of the antenna's performance characteristics under controlled conditions. This comprehensive testing confirms the antenna's performance across its operational bandwidth.

As demonstrated in Fig. 9(b), the AR bandwidth of the antenna is 17% within the frequency range of 5.75 GHz to 6.8 GHz. The minimum point of the AR aligns closely with the simulated values, although the measured bandwidth is somewhat narrower than predicted. This discrepancy can be attributed to a slight air gap that exists between the superstrate and the radiating patch, despite the use of low loss dielectric foam, which somewhat has impact on the test results. In addition, the simulation and measurement results of antenna gain are shown in Fig. 9(c). From the figure, it can be seen that the simulation results and actual measurement results are not completely consistent, which is due to the difficulty in reflecting the error caused by the SMA joint on the antenna during the actual measurement process in the antenna simulation. Moreover, as shown in Fig. 9(c), the simulated radiation efficiency of the antenna exceeds 90% within the operating frequency band.

Figure 10 illustrates the antenna's radiation pattern at frequencies of 6.0 GHz and 6.6 GHz. As illustrated in the figure, the left hand circularly polarized (LHCP) and right hand circularly polarized (RHCP) radiation patterns of the antenna are not entirely symmetrical. Based on the current distribution diagrams as mentioned earlier, the imbalance in current distribution on the driven patches and the MS results in incomplete symmetry of the LHCP and RHCP radiation patterns. The testing outcomes closely resemble the simulation data, confirming the antenna's effective performance. However, as highlighted in Fig. 11, due to limitations in the microwave anechoic chamber setup, the radiation pattern of the antenna could only be measured within a phase range of $-90°$ to $90°$. Despite these constraints, both the measurement and simulation results collectively validate the design's soundness and effectiveness.

FIGURE 11. Antenna measurement scene.

Finally, the comparison of the key results between the proposed antenna and the previously reported CP antennas is shown in Table 2. From Table 2, it can be seen that the proposed antenna performs well in terms of gain, radiation efficiency, impedance, and AR bandwidth.

4. CONCLUSION

A wideband CP patch antenna has been proposed in this paper. The antenna consists of a CP square-loop with sequential phase (SP) characteristics alongside four driven patches. This combination effectively excites multiple CP modes, merging them to achieve wide CP operational bandwidth. The proposed antenna has not only a wide 3 dB ARBW of 20% (6.29 GHz, 5.66–6.92 GHz), but also a wide IBW of 37.5% (5.97 GHz, 4.85–7.09 GHz). Additionally, the antenna maintains a consistent gain of 4.5–6.75 GHz within the CP operational bandwidth and is characterized by its low-profile design. The proposed antenna, given its features, is suitable for deployment in wideband wireless communication systems.

ACKNOWLEDGEMENT

This work is supported by the Key Natural Science Research Project of Anhui Higher Education Institutions: Research and application on electromagnetic regulation mechanism of artificial magnetic conductor materials 2022AH050070.

REFERENCES

[1] Feng, J., Z. Yan, S. Yang, F. Fan, T. Zhang, X. Liu, X. Zhao, and Q. Chen, "Reflect-transmit-array antenna with independent dual circularly polarized beam control," *IEEE Antennas and Wireless Propagation Letters*, Vol. 22, No. 1, 89–93, Jan. 2023.

[2] Chen, Z., W. Hu, Y. Gao, L. Wen, C. Li, Z. Hu, W. Jiang, and S. Gao, "Compact wideband circularly polarized loop antenna based on dual common and differential modes," *IEEE Antennas and Wireless Propagation Letters*, Vol. 21, No. 8, 1567–1571, Aug. 2022.

[3] Feng, D., H. Zhai, L. Xi, S. Yang, K. Zhang, and D. Yang, "A broadband low-profile circular-polarized antenna on an AMC reflector," *IEEE Antennas and Wireless Propagation Letters*, Vol. 16, 2840–2843, 2017.

[4] Sun, W., Y. Li, Z. Zhang, and Z. Feng, "Broadband and low-profile microstrip antenna using strip-slot hybrid structure," *IEEE Antennas and Wireless Propagation Letters*, Vol. 16, 3118–3121, 2017.

[5] Ding, K., C. Gao, T. Yu, D. Qu, and B. Zhang, "Gain-improved broadband circularly polarized antenna array with parasitic patches," *IEEE Antennas and Wireless Propagation Letters*, Vol. 16, 1468–1471, 2016.

[6] Wang, L., Z. Zhu, and Y. En, "Performance enhancement of broadband circularly polarized slot-microstrip antenna using parasitic elements," *IEEE Antennas and Wireless Propagation Letters*, Vol. 20, No. 12, 2255–2259, Dec. 2021.

[7] Ding, K., Y. Wu, K.-H. Wen, D.-L. Wu, and J.-F. Li, "A stacked patch antenna with broadband circular polarization and flat gains," *IEEE Access*, Vol. 9, 30 275–30 282, 2021.

[8] Ding, K., C. Gao, D. Qu, and Q. Yin, "Compact broadband circularly polarized antenna with parasitic patches," *IEEE Transactions on Antennas and Propagation*, Vol. 65, No. 9, 4854–4857, Sep. 2017.

[9] Li, M., Z. Zhang, M.-C. Tang, L. Zhu, and N.-W. Liu, "Bandwidth enhancement and size reduction of a low-profile polarization-reconfigurable antenna by utilizing multiple resonances," *IEEE Transactions on Antennas and Propagation*, Vol. 70, No. 2, 1517–1522, Feb. 2022.

[10] Zhu, H. L., S. W. Cheung, X. H. Liu, and T. I. Yuk, "Design of polarization reconfigurable antenna using metasurface," *IEEE Transactions on Antennas and Propagation*, Vol. 62, No. 6, 2891–2898, Jun. 2014.

[11] Ta, S. X. and I. Park, "Low-profile broadband circularly polarized patch antenna using metasurface," *IEEE Transactions on Antennas and Propagation*, Vol. 63, No. 12, 5929–5934, Dec. 2015.

[12] Yang, W., J. Zhou, Z. Yu, and L. Li, "Bandwidth- and gain-enhanced circularly polarized antenna array using sequential phase feed," *IEEE Antennas and Wireless Propagation Letters*, Vol. 13, 1215–1218, 2014.

[13] Hussain, N., M.-J. Jeong, A. Abbas, T.-J. Kim, and N. Kim, "A metasurface-based low-profile wideband circularly polarized patch antenna for 5G millimeter-wave systems," *IEEE Access*, Vol. 8, 22 127–22 135, 2020.

[14] Jia, Y., Y. Liu, S. Gong, W. Zhang, and G. Liao, "A low-RCS and high-gain circularly polarized antenna with a low profile," *IEEE Antennas and Wireless Propagation Letters*, Vol. 16, 2477–2480, 2017.

[15] Wong, K.-L., C.-C. Huang, and W.-S. Chen, "Printed ring slot antenna for circular polarization," *IEEE Transactions on Antennas and Propagation*, Vol. 50, No. 1, 75–77, Jan. 2002.

[16] Gao, X., G. Tian, Z. Shou, and S. Li, "A low-profile broadband circularly polarized patch antenna based on characteristic mode analysis," *IEEE Antennas and Wireless Propagation Letters*, Vol. 20, No. 2, 214–218, Feb. 2021.

[17] Liu, L., H. Chen, H. Sun, Z. Jin, L. F. Chernogor, D. O. Batrakov, T. Liu, and Z. Sun, "A broadband circularly polarized antenna based on transparent conformal metasurface," *IEEE Antennas and Wireless Propagation Letters*, Vol. 22, No. 12, 3197–3201, Dec. 2023.

[18] Behera, B., S. Mishra, M. H. Alsharif, P. Uthansakul, and M. Uthansakul, "A metasurface-inspired printed monopole antenna for 5G and RF energy harvesting application," *Engineering Science and Technology, An International Journal*, Vol. 51, 101638, Mar. 2024.

[19] Zhang, L., J. Chen, W. Wang, Z. Qi, and T. Ding, "Wideband single-fed circularly polarised patch antenna," *IET Microwaves, Antennas & Propagation*, Vol. 17, 1139–1144, Dec. 2023.

[20] Khan, I., K. Zhang, Q. Wu, I. Ullah, L. Ali, H. Ullah, and S. U. Rahman, "A wideband high-isolation microstrip MIMO circularly-polarized antenna based on parasitic elements," *Materials*, Vol. 16, 1–103, 2023.

[21] Mousavirazi, Z., H. Naseri, M. M. M. Ali, P. Rezaei, and T. Denidni, "A low-profile and low-cost dual circularly polarized patch antenna," *Progress In Electromagnetics Research Letters*, Vol. 107, 67–74, 2022.

[22] Aziz, R. S. and S. Koziel, "Circularly polarized metalens antenna design for 5G NR sub-6 GHz communication systems," *AEU — International Journal of Electronics and Communications*, Vol. 173, 155024, 2024.

[23] Guthi, S. and V. Damera, "High gain and broadband circularly polarized antenna using metasurface and CPW fed Lshaped aperture," *AEU — International Journal of Electronics and Communications*, Vol. 146, 154109, 2022.

[24] Kang, E., T. H. Lim, and H. Choo, "Design of a circularly polarized high-gain patch antenna using a higher-order mode with a heterogeneous substrate layer for GPS applications," *IEEE Access*, Vol. 11, 79 224–79 231, 2023.